UNIVERSIDAD NACIONAL AUTÓNOMA DE MÉXICO

FACULTAD DE INGENIERÍA

Monitoring detailed mangrove hurricane damage and early recovery using multisource remote sensing data.

ARTÍCULO ACADÉMICO

Para obtener el título de

Ingeniero Geomático

P R E S E N T A

Vizcaya Martínez Diego Arturo

ASESOR DE ARTÍCULO ACADÉMICO

Dr. Francisco Javier Flores de Santiago

Ciudad Universitaria, Cd. Mx., 2023

Journal of Environmental Management 320 (2022) 115830

Contents lists available at ScienceDirect

Journal of Environmental Management

journal homepage: www.elsevier.com/locate/jenvman

Research article

Monitoring detailed mangrove hurricane damage and early recovery using multisource remote sensing data

Diego Arturo Vizcaya-Martínez [a], Francisco Flores-de-Santiago [b,*], Luis Valderrama-Landeros [c], David Serrano [d], Ranulfo Rodríguez-Sobreyra [b], León Felipe Álvarez-Sánchez [e], Francisco Flores-Verdugo [f]

[a] Facultad de Ingeniería, Universidad Nacional Autónoma de México, A.P. 70-305, Av. Universidad 3000, Ciudad Universitaria, Coyoacán, Cd., México, 04510, Mexico
[b] Instituto de Ciencias del Mar y Limnología, Unidad Académica Procesos Oceánicos y Costeros, Universidad Nacional Autónoma de México, A.P. 70-305, Av. Universidad 3000, Ciudad Universitaria, Coyoacán, Cd., México, 04510, Mexico
[c] Subcoordinación de Percepción Remota, Comisión Nacional Para el Conocimiento y Uso de la Biodiversidad (CONABIO), 4903 Liga Periférico-Insurgentes Sur, Tlalpan, Cd., México, 14010, Mexico
[d] Facultad de Ciencias del Mar, Universidad Autónoma de Sinaloa, Paseo Clausen s/n, Mazatlán, 82000, Mexico
[e] Instituto de Ciencias del Mar y Limnología, Unidad de informática Marina, Universidad Nacional Autónoma de México, Universidad Nacional Autónoma de México, A. P. 70-305, Av. Universidad 3000, Ciudad Universitaria, Coyoacán, Cd., México, 04510, Mexico
[f] Instituto de Ciencias del Mar y Limnología, Unidad Académica Mazatlán, Universidad Nacional Autónoma de México, Av. Joel Montes Camarena s/n, Mazatlán, Sin., 82040, Mexico

ARTICLE INFO

Keywords:
DJI Phantom
Wind stress
Vegetation indices
Flooding
Mangrove fragmentation

ABSTRACT

Due to their location in tropical latitudes, mangrove forests are susceptible to the impact of hurricanes and can be vastly damaged by their high-speed winds. Given the logistic difficulties regarding field surveys in mangroves, remote sensing approaches have been considered a reliable alternative. We quantified trends in damage and early signs of canopy recovery in a fringe *Rhizophora mangle* area of Marismas Nacionales, Mexico, following the landfall of Hurricane Willa in October 2018. We monitored (2016–2021) broad canopy defoliation using 21 vegetation indices (VI) from the Google Earth Engine tool (GEE). We also mapped a detailed canopy fragmentation and developed digital surface models (DSM) during five study periods (2018–2021) with a consumer-grade unmanned aerial vehicle (UAV) over an area of 100 ha. Based on optical data from the GEE time series, results indicated an abrupt decline in the overall mangrove canopy. The VARI index was the most reliable VI for the mangrove canopy classification from a standard RGB sensor. The impact of the hurricane caused an overall canopy defoliation of 79%. The series of UAV orthomosaics indicate a gradual recovery in the mangrove canopy, while the linear model predicts at least 8.5 years to reach pre-impact mangrove cover conditions. However, the sequence of DSM estimates that the vertical canopy configuration will require a longer time to achieve its original structure.

1. Introduction

Mangrove forests thrive in the littoral zone of coastal lagoons and estuaries at tropical latitudes, and are thus subject to periodic damage caused by both the high-speed winds of hurricanes and the massive inundations resulting from storm surges (Kennedy et al., 2020). Although, different mangroves species have evolved with physiognomic adaptations to cope with these extreme events, they may present individual tree mortality or even some degree of canopy defoliation (broken branches and trunks) which can aggravate the overall canopy structure by creating gaps in the forest configuration (Krauss and Osland, 2020). Thereby it has been suggested that the extent of the damage to the mangrove forests depends on wind speed, duration, and direction (Simard et al., 2019). Moreover, and according to the severity of the hurricane, the subsequent recovery of the mangrove forest canopy may depend on species, forest structure (height, density, basal area), and possible hydrodynamic modifications (Serrano et al., 2020).

There are approximately 54 mangrove species worldwide, and each one presents specific responses to the damage caused by hurricanes. For instance, the black mangrove *Avicennia germinans* and the white

* Corresponding author.
E-mail address: ffloresd@cmarl.unam.mx (F. Flores-de-Santiago).

https://doi.org/10.1016/j.jenvman.2022.115830
Received 18 February 2022; Received in revised form 18 June 2022; Accepted 19 July 2022
Available online 6 August 2022

mangrove *Laguncularia racemosa* typically grow epicormic sprouts in response to canopy defoliation (Flores-Verdugo et al., 1992). Consequently, both species show lower mortality rates following high-speed wind damage (Tomlinson, 1994). On the contrary, the red mangrove, *Rhizophora mangle*, does not present epicormic growth because it lacks viable dormant buds in mature trunks and branches and is thus strongly susceptible to high degrees of mortality after hurricane impacts (Saenger, 2002). However, as *Rhizophora mangle* forests tend to present a high-density tree configuration in the understory (Arreola-Lizárraga et al., 2004), seedlings exhibit a rapid growth response when gaps are created by canopy defoliation (Krauss and Osland, 2020).

Considering the vast number of hurricanes that have impacted coastal areas worldwide during the last century (Krauss and Osland, 2020), it is surprising that only a few studies have examined the damage to mangroves and their overall recovery, for which a myriad of approaches have been used, such as field transects (Doyle et al., 1995; Imbert, 2018; Walcker et al., 2019; Fickert, 2020; Radabaugh et al., 2020), Google Earth images (Bashan et al., 2013), numerical models (Liu et al., 2013), *in situ* leaf area index (Feller et al., 2015), propagule dispersal (Kennedy et al., 2020), multi-proxy dataset (Yao et al., 2021), satellite-derived multispectral data (Han et al., 2018; Rivera-Monroy et al., 2019; George et al., 2021; McCarthy et al., 2021; Peereman et al., 2022), LiDAR (Gao and Yu, 2022), as well as unmanned aerial vehicles (Pennings et al., 2021; Serrano-Rubio et al., 2021). In summary, it has been suggested that mangrove trees may follow subsequent trajectories after a hurricane impact: regrowth of the surviving trees, recruitment of propagules, growth of seedlings in the understory, or complete degradation of the mangrove community caused by hydrological modifications.

In the Americas, mangrove forests are characterized by low diversity and are dominated by three species, which are distributed according to the hydroperiod (or flood regime) and microtopographic profile (Flores-Verdugo et al., 2018). This would make it unlikely for a damaged single-species mangrove community to be colonized by another species during the recovery stage (Félix-Pico et al., 2006). In theory, the recovery of a mangrove canopy will largely depend upon the growth of the same species, which may include new seedlings or seedlings that survived the wind damage at the understory (Doyle et al., 1995). As suggested by Ávila-Flores et al. (2020) and previously by Bashan et al. (2013), this situation is of utmost importance in mangroves of arid and semi-arid environments, which are under constant stress and have difficulty regenerating after disruptions by hurricanes.

The consequences of climate change, with special emphasis on the increase in sea surface temperature, have caused a ubiquitous trend towards atmospheric events globally (Nóbrega et al., 2016). This has made tropical coastal systems more prone to extreme flooding and high-speed wind damage from frequent hurricane impacts. Consequently, there has been an increasing need to monitor the early recovery of the mangrove canopy following the landfall of tropical storms and hurricanes worldwide. To this end, remote sensing techniques constitute a cost-effective approach (Kovacs et al., 2001).

Historically, the most common source of remote sensing data has been from spaceborne sensors with medium to high spatial resolution, such as the Landsat and Sentinel missions, which have been adapted for certain applications (Han et al., 2018). However, persistent cloud cover may be a hindrance when using passive data at tropical latitudes. In this respect, the use of modern technologies, such as unmanned aerial vehicles (UAV), has provided a suitable approach for target-specific environmental assessments due to their ultra-high spatial resolution (Flores-de-Santiago et al., 2020). Therefore, more robust and repeatable detection techniques must be developed using UAVs to improve the accuracy of mangrove species discrimination. We evaluated the hypothesis that canopy damage by high-speed winds and its subsequent early recovery rate will depend on the location and tree height of the mangrove species. The objective of this study was to quantify trends in canopy damage and signs of early recovery following the direct impact of Hurricane Willa by means of time series of satellite data and detailed canopy classification, combining orthomosaics and digital surface models (DSM) from a consumer-grade UAV.

2. Materials and methods

2.1. Study area

The Teacapán-Agua Brava-Las Haciendas estuarine mangrove complex, also known as Marismas Nacionales, is the most extensive estuarine system (170,000 ha) on the Eastern Pacific coast (Fig. 1a). It presents two direct connections to the adjacent Pacific Ocean: Teacapán, a natural channel at the north, and the Cuautla Canal at the south, which was constructed in 1972 and caused severe hydrological modifications (Serrano et al., 2020), which resulted in irreversible damage to the mangroves (Kovacs et al., 2013). Additionally, Isla La Palma, a large island, is located between the Teacapán channel and the Agua Grande lagoon (Fig. 1b) (Valderrama-Landeros et al., 2020). There are three dominant mangrove species throughout the estuarine system: *Avicennia germinans*, *Laguncularia racemosa*, and *Rhizophora mangle* (Kovacs et al., 2009). *Rhizophora mangle* is commonly found along main tidal channels and lagoons in narrow/dense clusters, while fragmented and dense stands of *Laguncularia racemosa* predominate in the south. Unlike the other two mangrove species, *Avicennia germinans* stands typically present a shrub (<2-m high) and dense configuration at the north section of the study site (Kovacs et al., 2013). Overall, the mangroves of this estuarine system present some degree of degradation due to hydrological modifications resulting from the construction of the Cuautla Canal (Kovacs et al., 2011; Serrano et al., 2020) and hydroelectric infrastructure throughout the 12 rivers (Valderrama-Landeros and Flores-de-Santiago, 2019).

The mangrove forest for our research is located along the edge of the estuary that surrounds the island of Isla La Palma (Fig. 1c). Kovacs et al. (2009) mapped the extent of mangrove conditions of this island using optical QuickBird satellite data and field data collected within the mangrove forests. They found that 40% of the 3040 ha were classified as dead stands, and only 8% were in pristine condition (i.e., fringe *Rhizophora mangle*). The remaining 52% was classified as an *Avicennia germinans* shrub, which is no more than 2-m height. Although mangrove services are harder to evaluate and thus tend to be underpriced, published quantitative data indicates that mangroves in this coastal system are of utmost importance for the food web structure and trophic dynamics of fish communities (Muro-Torres et al., 2019).

Hurricane Willa originated in the south coast of Mexico on October 19, 2018. On October 22 it reached category 5, the maximum category recorded on the Saffir-Simpson hurricane wind scale, as it crossed the Pacific Ocean at a wind speed of 259 km h^{-1} (https://coast.noaa.gov/). However, on October 23 it weakened into a category 3 and made landfall at Marismas Nacionales on the morning of October 24 with an average wind of ~100 km h^{-1} and maximum wind gusts of 185 km h^{-1}. The combined storm surge and a spring tide of 145 cm of amplitude at the time of impact (http://predmar.cicese.mx/calendarios/) resulted in unprecedented inundation levels for Marismas Nacionales. For example, we observed a clear change in the flooding regime between the two enhanced false-color Sentinel-2 composites (Near-infrared, Red, and Green) five days before the hurricane on October 18, 2018, and four days after the impact on October 28, 2018 (Fig. 2). Moreover, time-series satellite data (NOAA) recorded maximum precipitation of 70 mm during the landfall of Hurricane Willa. At the same time, the Acaponeta river gauge station showed a water level of 4 m (Fig. 2).

Following is a list in chronological order of the tropical storms and hurricanes in a 50-km radius that have made landfall at the north section of Marismas Nacionales: tropical storm Norman in September 2000, with a maximum wind speed of 50 km h^{-1}; hurricane category 2 Rosa in October 1994 (167 km h^{-1}), hurricane category 3 Tico on October 1983 (203 km h^{-1}), tropical storm Adolph on May 1983 (65 km h^{-1}), tropical

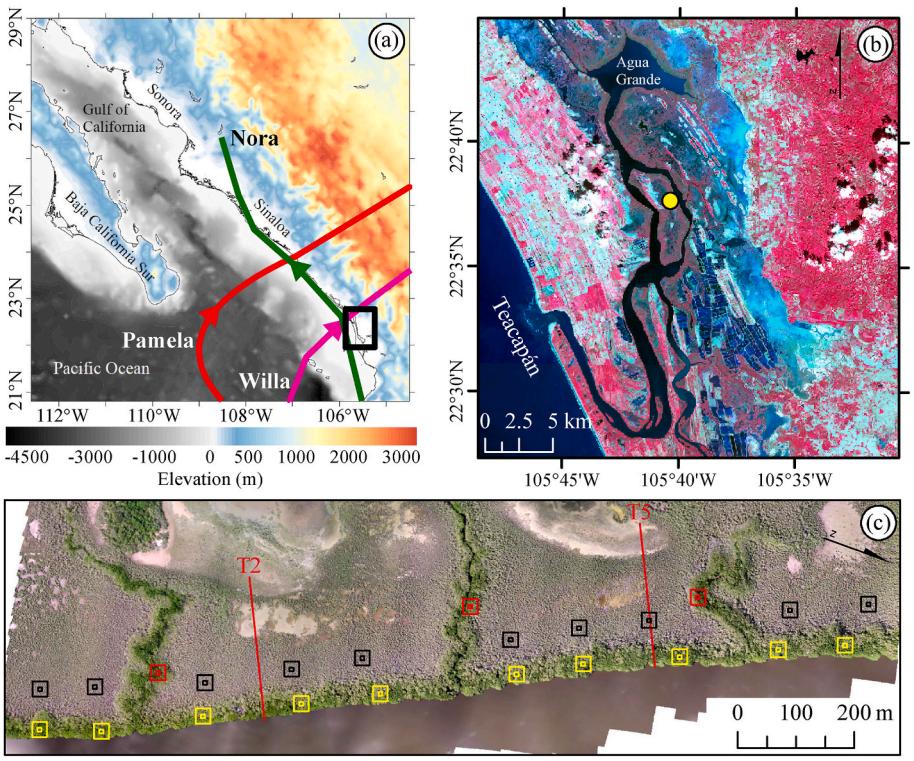

Fig. 1. (a) Digital elevation model (m) of the northwestern coast of Mexico based on freely available TOPEX data (https://topex.ucsd.edu/cgi-bin/get_data.cgi). The black rectangle indicates the Location of Marismas Nacionales. The magenta vector shows the center of Hurricane Willa's path on October 23–24, 2018. The green and red vectors indicate the track of Hurricanes Nora and Pamela in late 2021, respectively. (b) The Isla Palma location between the Agua Grande lagoon and the Teacapán mouth at the North section of the Marismas Nacionales wetland system (Enhanced Near-infrared, Red, Green of Sentinel-2 dated November 22, 2019). The yellow circle indicates the location of the surveyed area by the UAV (c). The yellow, black, and red squares show the positions of the Google Earth Engine pixels extracted for the *Rhizophora mangle* fringe, *Avicennia germinans* shrub, and *Rhizophora mangle* basin, respectively. Large squares represent the Landsat-8 area, while small squares indicate the Sentinel-2. The red lines depict the path of the two vertical transects (T2 and T5). (For interpretation of the references to color in this figure legend, the reader is referred to the Web version of this article.)

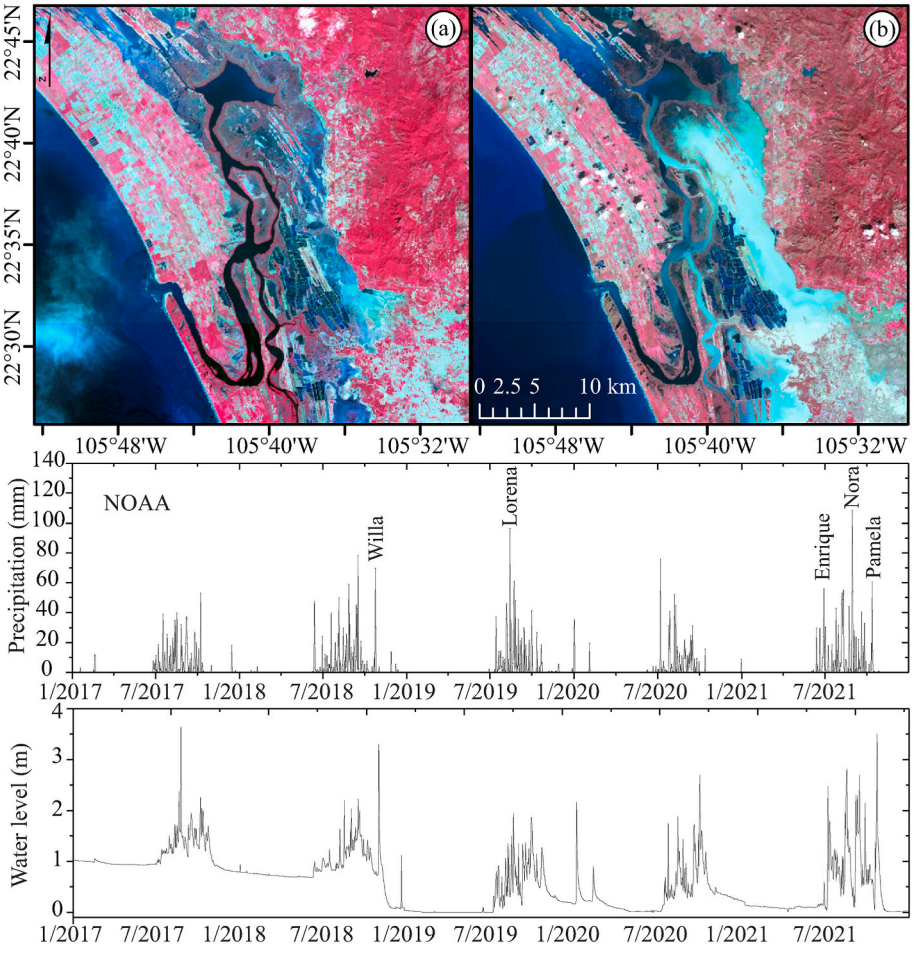

Fig. 2. (a) Enhanced false-color Sentinel-2 composite (Near-infrared, Red, and Green) acquired five days before hurricane Willa's landfall on October 18, 2018, and (b) four days after on October 28, 2018. Time series of the precipitation (NOAA) and the Acaponeta river water level (CONAGUA) from January 2017 to December 2021. The date of the impact of major tropical storms and hurricanes is indicated within the graph. (For interpretation of the references to color in this figure legend, the reader is referred to the Web version of this article.)

storm Otis on October 1981 (100 km h^{-1}), hurricane category 3 Olivia on October 1975 (185 km h^{-1}), tropical storm Eileen on June 1970 (65 km h^{-1}), and tropical storm Hazel on September 1965 (80 km h^{-1}) (https://coast.noaa.go/). Hence, the estuarine complex of Marismas Nacionales tends to experience the impact of at least one major hurricane every decade.

2.2. Wind speed data

We extracted and plotted the vector time series $\overrightarrow{V}(u,v)$ and the wind speed magnitude $\sqrt{u^2+v^2}$ with the sole purpose of analyzing the atmospheric conditions before the impact of Hurricane Willa. Specifically, we obtained and modeled the wind components *u* and *v* every 6 h at an altitude of 20 m from the ground at 22° N and 106° W from January 2018 to December 2021 according to the Navy Global Environmental Model (NAVGEM) through the NOAA server (https://coastwatch.pfeg.noaa.gov/erddap/griddap/index.html?page=1&itemsPerPage=1000).

2.3. Google Earth Engine time series

We selected a total of 23 field locations representing the *Rhizophora mangle* fringe condition (10 pixels), the *Avicennia germinans* shrub condition (10 pixels), and the *Rhizophora mangle* basin condition (3 pixels). We recorded the central location of each sampling point using a global positioning system (GPS), with an error of less than 1 m. On each location, we extracted bands 2 (blue), 3 (green), 4 (red), and 5 (near-infrared) of the Landsat-8 (OLI) over six years (3 pre- and 3 post-Willa). In addition to the previously mentioned satellite bands, we obtained bands 5 (Red Edge 1), 6 (Red Edge 2), 7 (Red Edge 3), 11 (SWIR1), and 12 (SWIR2) from the Sentinel-2 data collection over four years (1 pre- and 3 post-Willa). We performed the overall analysis using the built-in Google Earth Engine (GEE) tool installed on the Quantum GIS V. 3.16.13 software. Detailed information on the principle of this approach can be found in Valderrama-Landeros et al. (2021). There is a considerable number of vegetation indices (VI) that have used RGB, red edge (RE), and near-infrared (NIR) data (e.g., Hatfield and Prueger, 2010; Neupane et al., 2019; Stary et al., 2020; Zhou et al., 2021). However, and based on phenological studies of mangroves (Zhu et al., 2017; Mafi-Gholami et al., 2019; Valderrama-Landeros et al., 2021), we selected 13 RGB and 8 NIR-RE indices, including three VI exclusively developed for mangrove assessments (Table 1).

Table 1
Equations for visible (RGB), red edge (RE), near-infrared (NIR), and short-wave infrared (SWIR) vegetation indices used in this study.

Type	Vegetation Index	Equation	Reference
NIR RE	Normalized Difference Vegetation Index (NDVI)	NIR-R/NIR + R	Rouse et al. (1973)
	Red Edge Normalized Difference Vegetation Index ($NDVI_{re}$)	NIR-RE_1/NIR + RE_1	Gitelson and Merzlyak (1994)
	Chlorophyll Index Red Edge (CIg-re1)	RE_1/G-1	Gitelson et al. (2003)
	Chlorophyll Index Red Edge (CIg-re2)	RE_2/G-1	Gitelson et al. (2003)
	Chlorophyll Index Red Edge (CIg-re3)	RE_3/G-1	Gitelson et al. (2003)
	Combined Mangrove Recognition Index (CMRI)	NDVI-(G-NIR/G + NIR)	Gupta et al. (2018)
	Normalized Difference Mangrove Index (NDMI)	$SWIR_2$-G/$SWIR_2$+G	Shi et al. (2016)
	Modular Mangrove Recognition Index (MMRI)	|G-$SWIR_1$/G + $SWIR_2$|-|NDVI|/|G-$SWIR_1$/G + $SWIR_2$|+|NDVI|	Diniz et al. (2019)
RGB	Visual Atmospheric Resistance Index (VARI)	G-R/G + R–B	Gitelson et al. (2002)
	Triangular Greenness Index (TGI)	(G-0.39) (R-0.61) B	Hunt et al. (2011)
	Excess Green Index (ExG)	2G-R-B	Woebbecke et al. (1995)
	Vegetation Index (VEG)	$G/R^{0.67}B^{0.33}$	Torres-Sanchez et al. (2014)
	Color Index Vegetation (CIVE)	0.44R-0.88G+0.39B + 18.79	Guerrero et al. (2012)
	Normalized Green-Red Difference Index (NGRDI)	G-R/G + R	Torres-Sanchez et al. (2014)
	Normalized Green-Blue Difference Index (NGBDI)	G-B/G + B	Du et al. (2017)
	Visible-Band Difference Vegetation Index (VDVI)	2G-R-B/2G + R + B	Du et al. (2017)
	Red-Green Ratio Index (RGRI)	R/G	Wan et al. (2018)
	Blue-Green Ratio Index (BGRI)	B/G	Calderon et al. (2013)
	Woebbecke Index (WI)	G-B/R-G	Woebbecke et al. (1995)
	Red-Green-Blue Ratio Index (RGBRI)	R + B/2G	Xie et al. (2020)
	Red-Green-Blue Vegetation (RGBVI)	G^2-(R*B)/G^2+(R*B)	Bendig et al. (2015)

2.4. UAV flight missions, data collection, and analysis

We acquired sequences of UAV images in October 2018 (before the impact) and November 2018, 2019, 2020, and 2021, utilizing a rotary-wing DJI Phantom series quadcopter and its built-in visible camera. We configured flight missions using the autopilot software Map Pilot V. 2.0.1 over an area of 100 ha, following the criteria by Flores-de-Santiago et al. (2020). The inexpensive navigation system triggered the UAV camera (nadir view) at a specific time interval of 2 s per image and recorded the UAV location at the center of the instant field-of-view. Image-capture orientation and altitude were automatically recorded and stored in the flight log file (.csv) by the onboard internal measurement unit (IMU) and GPS.

We radiometrically calibrated all individual images using pre-flight white and black targets deployed at the control base station. Once the acquired images were saved on the computer, we used Agisoft Metashape software V. 1.5.2 (http://www.agisoft.com/) to generated orthorectified images and DSM. Although there are several available photogrammetric programs, Agisoft has provided the best results in terms of quality and photogrammetric products (Sona et al., 2014). Overall, the whole automatic process involved three main stages: (1) image alignment, (2) dense cloud construction, and (3) orthoimage/DSM generation. We measured the height of the mangrove classes in the field with a portable Vertex Laser VL400 hypsometer as described by Flores-de-Santiago et al. (2020). We performed all the computer processing on the same workstation, an ASUS G751J with an Intel 8 Core i7 (2.6 GHz), 32 GB of RAM, and an NVIDIA GeForce GTX 980M graphic card.

Based on the GEE time series results, we selected the most suitable RGB VI to discriminate between *Rhizophora mangle* and *Avicennia germinans*. RGB VI is the only available option because the UAV consumer-grade camera does not provide a full multispectral data range. However, RGB VI has been used for this type of spatial data with promising results regarding precision agriculture (Zhang et al., 2019) and overall mangrove phenology trends (Valderrama-Landeros et al., 2021). Following the selection of the optimal VI, we performed a decision tree analysis for the classification of *Rhizophora mangle*, *Avicennia germinans*, open water, and saltpan on ArcMap software V. 10.2.2 following the recommendations by Flores-de-Santiago et al. (2013a) and Zhou et al. (2021). We performed an automatic vectorization with the pixel values selected for the *Rhizophora mangle* and *Avicennia germinans* classes. In

the absence of NIR data, we applied manual elimination in case some vectors represented shadows (Flores-de-Santiago et al., 2018). We quantified the individual vectors (i.e., objects) and the overall canopy area for each of the five orthomosaics.

3. Results

3.1. Wind impact on Marismas Nacionales

The wind magnitude and direction between 2018 and 2021 show an abrupt increase in wind speed during tropical storms and hurricanes (Fig. 3), in which Hurricane Willa recorded the strongest wind gusts and an averaged wind speed of 104 km h^{-1}. The mangroves were under the influence of these maximum wind gusts for 31 h, followed by 23 h of wind speeds twice the average recorded under no-hurricane conditions.

The seven recorded tropical storms and hurricanes showed a similar NNE-NNW wind direction. Specifically, hurricane category 1 Pamela in October 2021 (120 km h^{-1}), hurricane category 1 Nora in August 2021 (140 km h^{-1}), hurricane category 1 Enrique in June 2021 (150 km h^{-1}), tropical storm Hernan in August 2020 (75 km h^{-1}), hurricane category 4 Genevive in October 2020 (215 km h^{-1}) –although this hurricane was located at 249 km from the study site and thus the wind speed recorded in Fig. 3 is ~30 km h^{-1}–, and Hurricane category 1 Lorena in September 2019 (140 km h^{-1}). The average wind speed and maximum wind magnitude between 2018 and 2021 were 12.7 km h^{-1} and 35.5 km h^{-1}, respectively.

3.2. VI time series from Landsat-8 and Sentinel-2 data

The Landsat-8 VI time series extracted from the GEE for the fringe *Rhizophora mangle*, *Avicennia germinans* shrub, and *Rhizophora mangle* basin classes are shown in Fig. 4. We could not use RE information for the Landsat-8 series because such a sensor lacks an RE band. Among the remaining 18 VIs, the NDVI continues to be the most useful index in terms of the overall mangrove trend, showing an abrupt negative change in their tendency after the impact of Hurricane Willa. While there was a clear difference in the NDVI trend between the *Rhizophora mangle* (fringe and basin) and the *Avicennia germinans* before the hurricane landfall, the

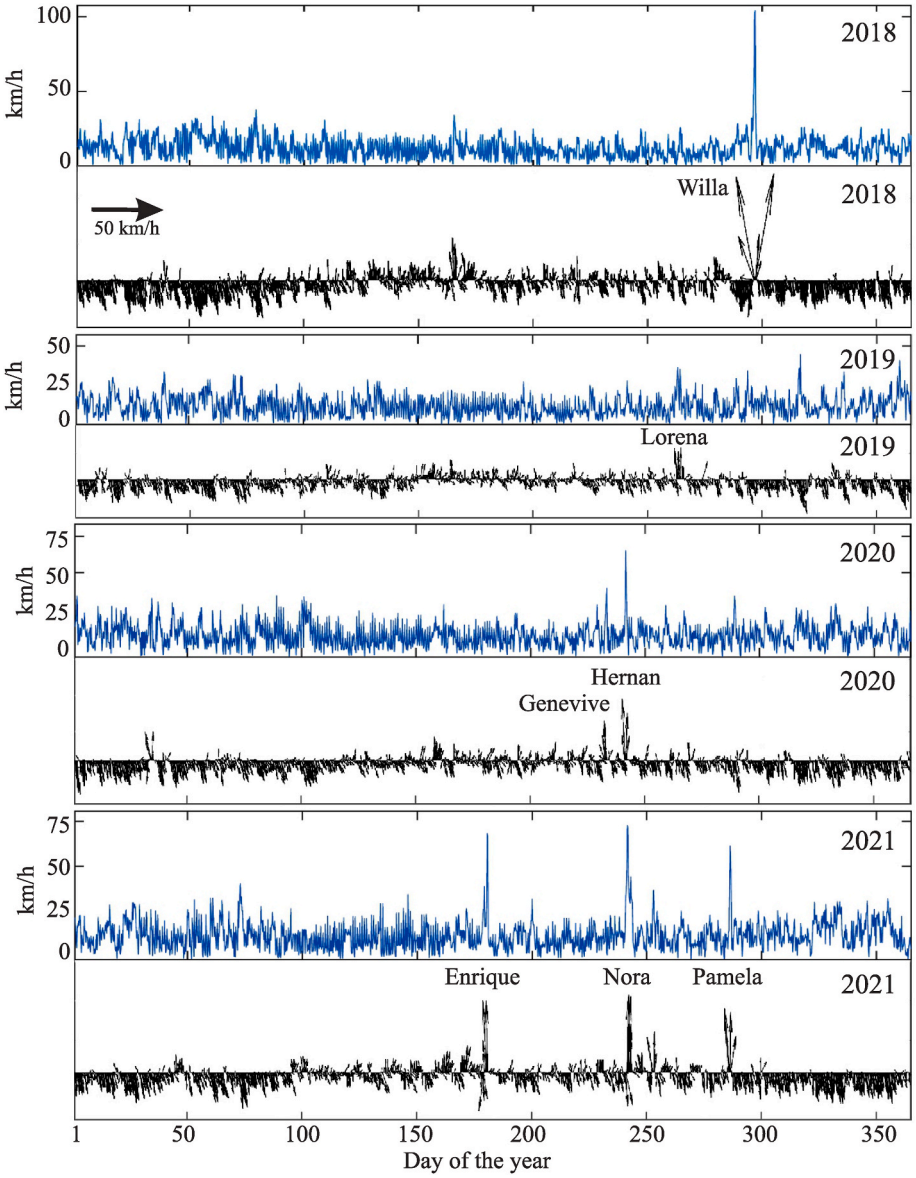

Fig. 3. Time series of the wind speed (blue) and wind direction (black vectors) from January 2018 to December 2021. Data was acquired from the Navy Global Environmental Model. The date of the impact of major tropical storms and hurricanes is indicated within the graph. (For interpretation of the references to color in this figure legend, the reader is referred to the Web version of this article.)

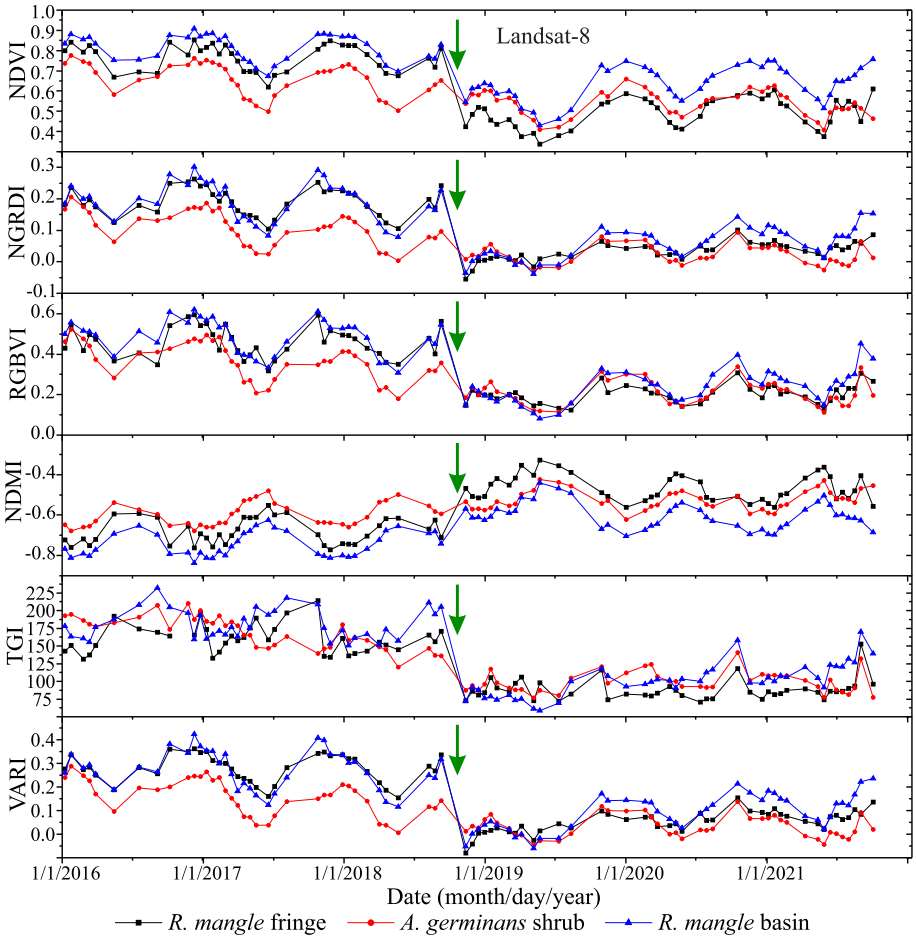

Fig. 4. Time series of vegetation indices extracted from the Google Earth Engine platform for the Landsat-8 data. The green arrows indicate the date of the impact of Hurricane Willa. (For interpretation of the references to color in this figure legend, the reader is referred to the Web version of this article.)

difference after the impact between the fringe *Rhizophora mangle* and basin conditions is now substantial, with the basin class presenting higher index values.

On the other hand, the lowest NDVI corresponds to the *Rhizophora mangle* fringe class, which is now similar to the overall *Avicennia germinans* pattern. Surprisingly, the mangrove index (NDMI) did not show a clear tendency. Among the eight RGB VIs, only the NGRDI, RGBVI, TGI, and VARI showed a similar trend when compared to the VIs that used a multispectral NIR band. Among the most useful RGB indices, the VARI index was capable of separating *Avicennia germinans* from the rest of the *Rhizophora mangle* classes. Furthermore, the VARI index was able to discriminate between both *Rhizophora mangle* classes throughout the year 2021, even though the separation between these two mangrove classes was not as good as the NDVI.

As expected, the Sentinel-2 time series, which now incorporates new RE indices, showed similar results compared to the Landsat-8 data (Fig. 5). For instance, the NDVI depicted the same pattern, with the *Rhizophora mangle* basin higher than both the fringe *Rhizophora mangle* and the *Avicennia germinans* classes. Therefore, it appears that the *Rhizophora mangle* fringe class was the one most affected by the impact of the hurricane. However, there has been an apparent recovery of the mangrove cover area, at least for the *Rhizophora mangle* classes. Interestingly, we did not observe a difference between the NDVI, the $NDVI_{Red\ Edge}$, and the Cig-re2 indices. The same situation was found between the CMRI mangrove index and the RE indices. Regarding the latter, the VARI and NGRDI showed a similar trend compared to the NDVI; however, unlike the NGRDI, the VARI was able to separate the two classes of *Rhizophora mangle*.

3.3. Orthomosaics and DSM from the UAV data

According to the trends depicted in Figs. 4 and 5, we selected the VARI index as the most suitable one to classify mangrove species with RGB data from the UAV. As previously found, there are some caveats that concern the validity of the assessment results regarding discrimination between both *Rhizophora mangle* classes using RGB data. In this sense, and based on the overall VARI index trend, we decided to merge both red mangrove classes into a single *Rhizophora mangle* group. Fig. 6 shows a representative area of the 100-ha surveyed site during the five UAV missions at Isla Palma. From left to right, true color orthomosaic, decision tree classification using the VARI index, and modeled DSM. The mapped area represents a typical semi-arid intertidal environment where *Rhizophora mangle* trees are distributed adjacent to the coastal lagoon and along the small tidal channels through the interior of the island. *Avicennia germinans* shrubs are distributed in more inland areas where the hydroperiod is less intense and where they are thus under considerable hydric stress.

All five orthomosaics present similar light conditions because they were recorded at practically the same hour of the day and during the same month. The VARI index was able to separate *Rhizophora mangle* (red coloration) from *Avicennia germinans* (orange coloration) and other land features, such as open water and saltpan (white coloration) (Fig. 6). The ultra-high spatial resolution of the UAV provided the possibility of determining the defoliated areas. Moreover, it was possible to capture the location of the fallen trees after the hurricane's landfall and quantify early signs of mangrove recovery, a situation that is not that feasible with conventional satellite images (e.g., Landsat-8 and Sentinel-2).

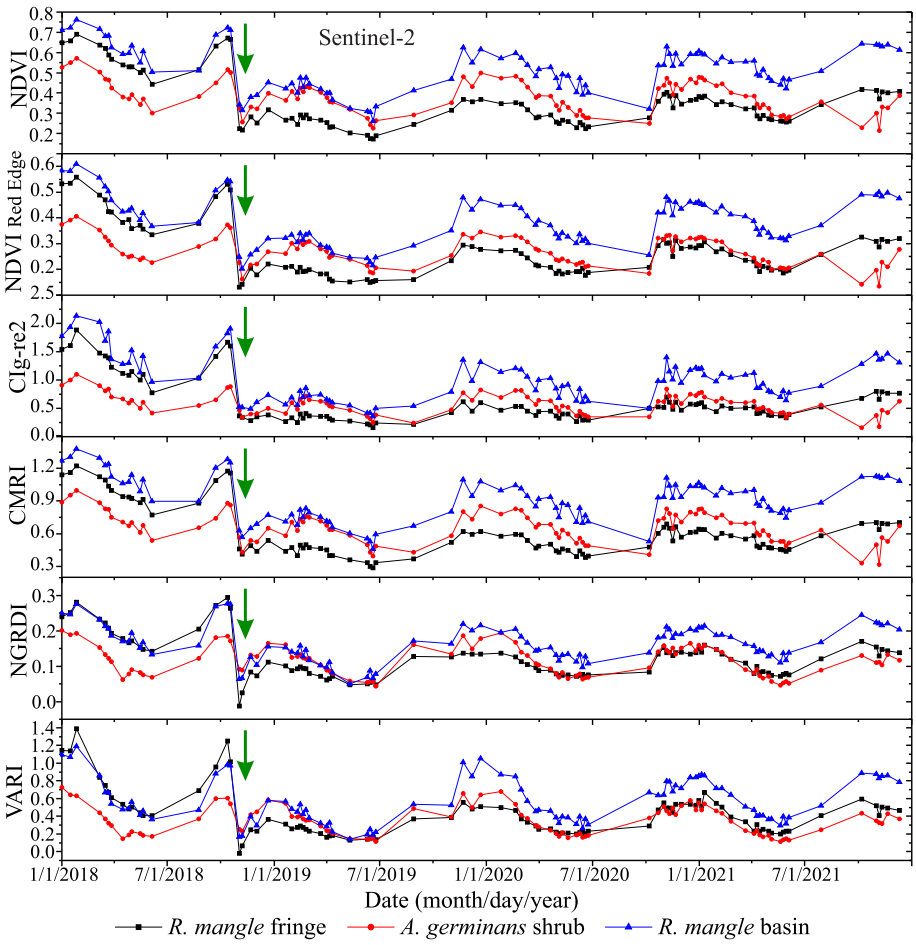

Fig. 5. Time series of vegetation indices extracted from the Google Earth Engine platform for the Sentinel-2 data. The green arrows indicate the date of the impact of Hurricane Willa. (For interpretation of the references to color in this figure legend, the reader is referred to the Web version of this article.)

Regarding the DSM, the *Rhizophora mangle* depicted a monospecific configuration before the hurricane's impact (October 16, 2018). Although some trees had survived on November 16, 2018 —three weeks after the landfall— there were many recorded defoliated 8 to 12-m high trunks. These dead trunks were rapidly lost two years after the event, as seen in November 2020. Many new trees/seedlings have been colonizing the area, as shown on the orthomosaic and DSM in November 2021. Overall, the RGB mosaic and the corresponding VARI index classification show a positive recovery of what looks like mangrove leaf growth; nevertheless, the DSM shows that the surviving trees are relatively short compared to the original canopy configuration. There was confirmation in the field that most of the fringe *Rhizophora mangle* trees presented some inclination and thus less height.

The vertical DSM profile of transect T2 illustrates an area that has been under constant recovery since the impact, while transect T5 depicts permanent damage (Fig. 7). Both transects present a similar canopy profile before the impact of Hurricane Willa with a maximum tree height of 13 m for the *Rhizophora mangle* fringe class. The *Avicennia germinans* stands showed a typical shrub configuration (2–4 m high) before the event. Following the hurricane's high-speed winds, both locations exhibited massive damage regarding the vertical canopy profile. In essence, most of the tallest trees (9–13 m) were defoliated, and only a few trees with a height of less than 8 m survived. For example, a few trees survived and started growing through transect T2, while we found considerable open areas within the canopy and several remnants of dead trunks through transect T5. The photographs in the field were taken in November 2021, three years after the hurricane's impact. Specifically, many trees presented some inclination towards the open water, and it became common to see a relatively recovered *Rhizophora mangle* fringe community (7.9–11.6 m high) in front of transect T2 with some dead trunks in the back (8.7–10.9 m high). It was also common to find individual trees that had lost the original thick canopy configuration and that had started to develop leaves through the trunk, as seen in the photograph at T2. On the other hand, no apparent recovered area was depicted in the field photographs in front of transect T5. Although this situation has not been commonly found through the study site, we believe the T5 transect depicts an unsuccessful natural recovery stage for reasons that must be investigated. We found only a few remnants of *Rhizophora mangle* between 2.8 and 4.4 m; however, there were also a considerable number of dead trunks of this species (6.1–12.6 m height).

The overall accuracy achieved for the vectorized clusters of the *Rhizophora mangle* class within the five orthomosaics fluctuated between 92 and 95%. These results had been expected because the analysis was based on a single mangrove thematic class. The original orthomosaic from October 2018 showed a total area of 10.9 ha distributed in 60 individual clusters (Fig. 8). From these polygons, only 2.4 ha of canopy remained after the hurricane landfall, distributed into 683 sparse clusters and representing an approximately canopy loss of 78%. Subsequently, the recorded canopy recovery areas were 4.1 ha in 2019, 4.9 ha in 2020, and 5.8 ha in 2021. After three years, the overall *Rhizophora mangle* cover area was 53% compared to the original condition. Using linear analysis, we contrasted the last four years of canopy structure and found the following linear equation: canopy area = 1.1 (years)+1.55 with an R^2 of 0.96. Therefore, although it may be predicted that it will take approximately 8.5 years to reach an original area of 10.9 ha, there are still some remaining gaps within the canopy that may take more time

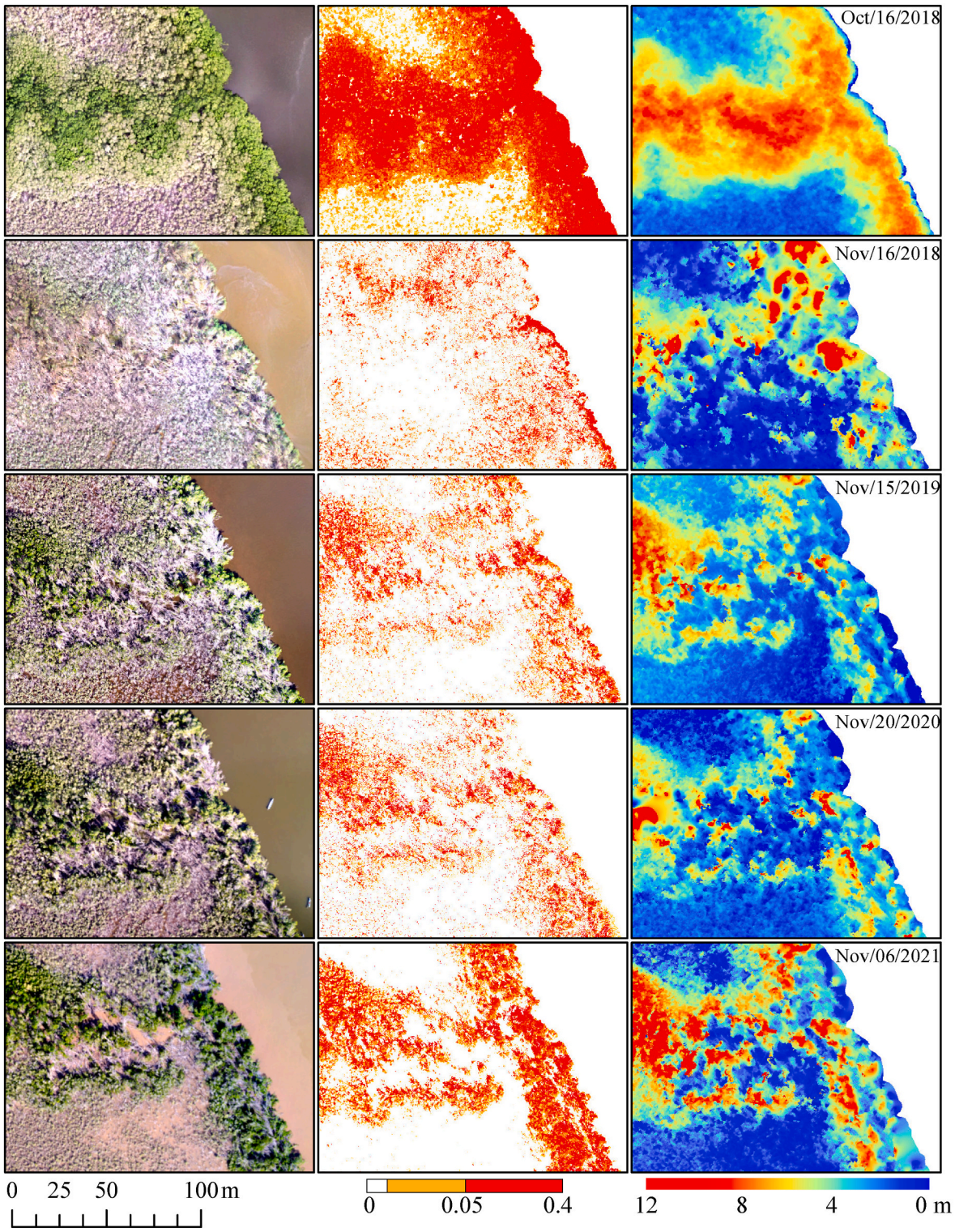

Fig. 6. Characteristics portrayals of the *Rhizophora mangle* and *Avicennia germinans* vegetation for the five UAV data collections. From left to right: the original UAV orthomosaic (RGB), the Visible Atmospherically Resistant Index (VARI), and the digital surface model (m).

for it to fully achieve its pre-hurricane condition.

4. Discussion

The synergy between freely available time series of VI from the GEE platform and the spatial and vertical variability assessed with ultra-high spatial resolution orthomosaics/DSM from UAV was successful in analyzing the temporal, spatial, and vertical distribution of the mangrove canopy after the landfall of massive Hurricane Willa in October 2018. Despite the tropical storms and hurricanes that have traveled close to the study site after Hurricane Willa, such atmospheric events have been less intense, as their landfall has been at a relative distance from the study site. Hence, the probability of further mangrove canopy damage to the same assessed area has been minimal.

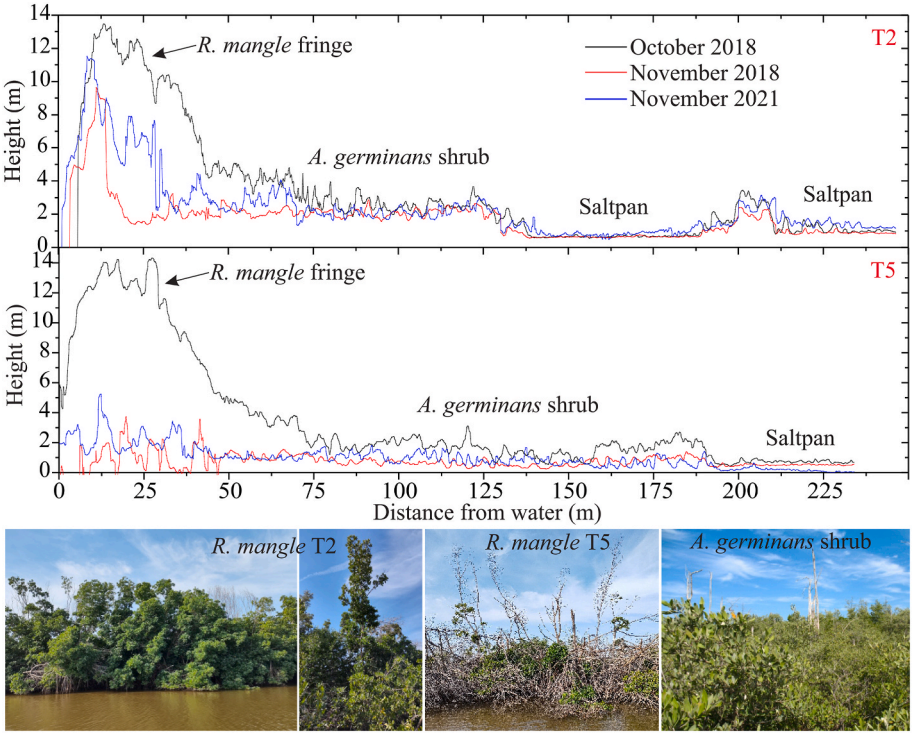

Fig. 7. Vertical profiles of the two representatives transect at Isla Palma extracted from the UAV digital surface models. The colored lines indicate the vertical profiles before the impact (October 2018), after the impact (November 2018), and three years post-hurricane (November 2021). Examples of field photos taken in November 2021. From left to right: recovered *Rhizophora mangle* fringe condition in front of transect T2, a single *Rhizophora mangle* tree that survived the hurricane impact, degraded *Rhizophora mangle* in front of transect T5, and *Avicennia germinans* shrub condition.

4.1. Satellite data time series

The three mangrove classes (*Rhizophora mangle* fringe, basin, and *Avicennia germinans* shrub) presented a notable change in canopy defoliation after the impact of Hurricane Willa. For example, both Landsat-8 and Sentinel-2 series showed that the less affected class, in terms of canopy changes, was the *Avicennia germinans* shrub. We expected this pattern because of its 2–4 m height, given that large trees, such as the fringe *Rhizophora mangle* (8.5–13 m), are often more susceptible to damage during adverse wind events (Doyle et al., 1995). Moreover, only those *Rhizophora mangle* trees with a height of less than 8 m survived within the fringe community. Radabaugh et al. (2020) found that larger trees are more vulnerable to damage than mangrove shrubs during storm events because of the strong wind intensity. These authors also consider that the degree of branch damage in trees is a key factor in explaining delayed mortality, as such alterations in defoliation and loss of branches may increase stress and eventual mortality. Another study by Kovacs et al. (2001) in the same study site points out that approximately 80% of the taller trees with a diameter greater than 20 cm were dead, in contrast to only 16% of the shrub mangroves (diameter of 2.5–5 cm). In 2019 we also found a considerable number of established *Rhizophora mangle* seedlings. There is the possibility that the 13-m high fringe *Rhizophora mangle* acted as a shield and protected both the understory *Rhizophora mangle* saplings and the adjacent *Avicennia germinans* from the wind gusts. Previous studies, such as those by Fickert (2020) and Serrano-Rubio et al. (2021), have shown that direct planting after a hurricane is not necessary for a mangrove forest to recover naturally if the hydrological conditions have not changed since the impact. However, it has been suggested that the broken branches and dead trunks could uproot the newly established seedlings, thus extending the period of considerable colonization of the understory to more than four years in some locations (Flores-Verdugo et al., 1987). The temporal pattern in the mangrove canopy is expected because, as mentioned, the severity of hurricane impacts to the mangrove forest canopy and structure depends primarily on the maximum sustained wind speed (Imbert, 2018).

Marismas Nacionales is considered an impacted estuarine system because of hydrological modifications during the last decades (Serrano et al., 2020). Such adverse environmental conditions have caused a non-optimal development of the mangroves throughout the lagoons and tidal channels (Kovacs et al., 2013). The fringe *Rhizophora mangle* forest located at the northern section, where the hurricane made landfall, is considered a less vigorous forest compared to the same species at the Agua Brava lagoon in the south. Valderrama-Landeros et al. (2020) used Sentinel-2 images and observed a considerable decrease in the NIR wavebands at locations near Isla Palma. Hence, damage and defoliation to the mangrove canopy in other species, such as *Laguncularia racemosa*, can be expected to differ from the overall trend in the VI time series.

4.2. Visible UAV data

Regarding UAV limitations, it is well known that expensive multispectral cameras, the impossibility of obtaining digital elevation models (DEM) from passive sensors throughout the canopy, and minimal flight time are the main hindrance for wetland vegetation assessments (Flores-de-Santiago et al., 2020). Regarding the DSM from the UAV, we expected to find some discrepancy between the DSM obtained in our analysis and the actual DEM when using an active sensor such as LiDAR. However, the profiles revealed that the saltpan, which does not present vegetation, showed a similar height among the DSM models. Moreover, a relatively flat terrain within the fringe *Rhizophora mangle* is to be expected. Flores-Verdugo et al. (2018) used micro-topographic profiles and found that the difference between the *Avicennia germinans* and *Rhizophora mangle* was about 40 cm, which is relatively irrelevant when compared to a 13-m high canopy.

Not surprisingly, most mangrove studies have only focused on small areas when assessing environmental data with UAV platforms. Specifically, the assessed areas have been from 1 to 10 ha (Cao et al., 2019; Otero et al., 2018; Ruwaimana et al., 2018; Wang et al., 2020) to 30–85 ha (Guo et al., 2017; Li et al., 2019; Liu and Wang, 2018), with only two studies having encompassed relatively larger areas of 138 ha (Yu et al., 2017) and 260 ha (Zhu et al., 2019). One alternative could be to use fixed-wing UAVs, but such platforms are not easily deployed on small boats, especially during landing operations within coastal lagoons with

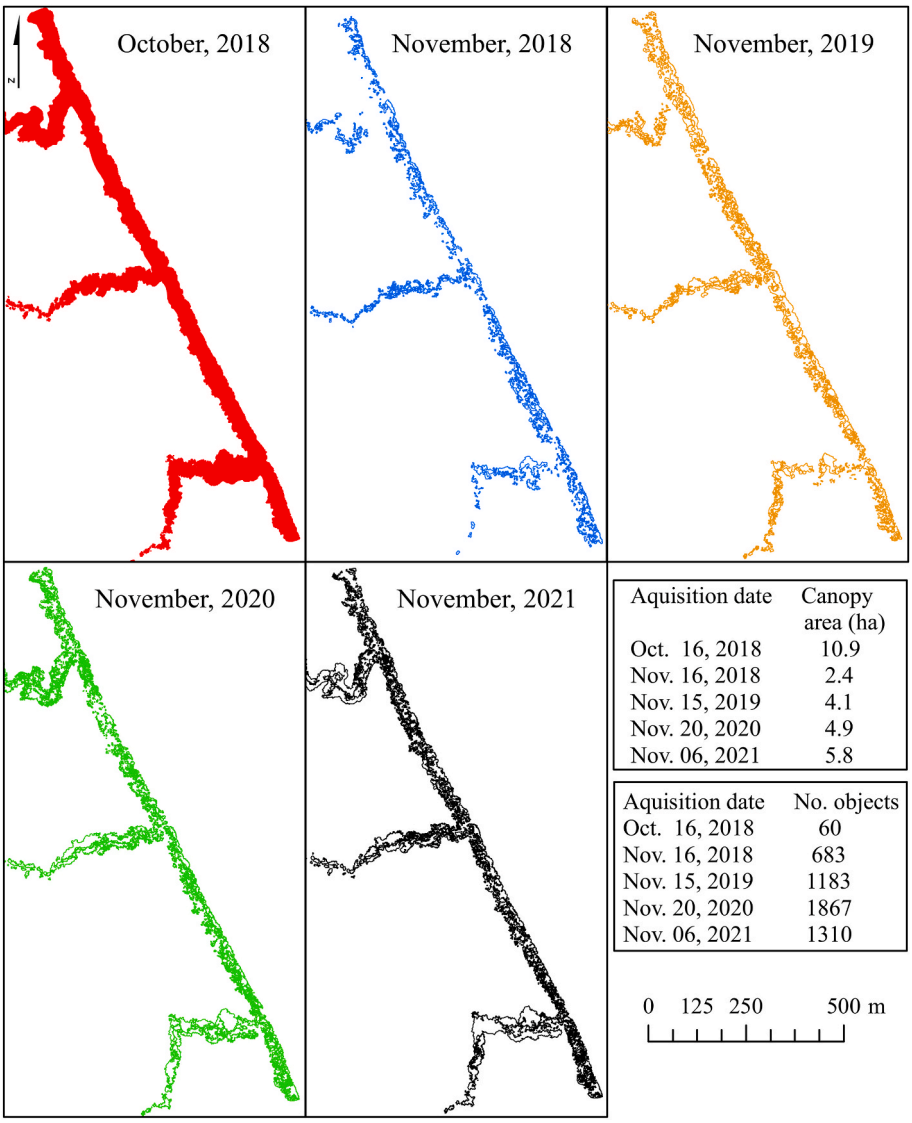

Fig. 8. The *Rhizophora mangle* canopy areas (ha) and the number of objects (continuous clusters) extracted from the five orthoimages using the Visible Atmospherically Resistant Index (VARI).

saltwater. However, new UAV developments of hybrid tail-sitter platforms, such as the Wingtra One (Wingtra AG, Zurich), enable image collection of areas up to 400 ha in a single flight (Oldeland et al., 2020), although the cost of this platform is expensive with respect to the traditional Phantom series. For example, the cost of the Phantom is only ~10% compared to the base cost of the Wingtra One after importation and taxes fees in Mexico.

To understand which VI could be feasible for mangrove canopy discrimination, we must keep in mind that we are using the inexpensive built-in RGB sensor that does not provide multispectral data, and that neither RE nor NIR bands are available in our orthomosaics. Hence, in the absence of validation data, such as spectroradiometers deployed in the field (e.g., Zhang et al., 2014; Flores-de-Santiago et al., 2013b), we use multispectral satellite VI-based data from the GEE time series for mangrove canopy assessments (Valderrama-Landeros et al., 2021). Even though this could be considered a heuristic approach, we believe that the positive and similar trend between the multispectral and RGB VIs from both Landsat-8 and Sentinel-2 time series could help us determine if the RGB VI from the UAV is suitable for mangrove classification purposes.

Despite the large availability of newly developed VI, the NDVI is by far the most widely used index regarding mangrove assessments and has provided reliable results concerning mangrove phenology (Valderrama-Landeros et al., 2021) and degradation (Valderrama-Landeros et al., 2018). Given the similarity between the VARI and the NDVI trends for both satellite platforms, we believe that the use of the VARI index could be a reliable alternative to sophisticated and expensive multispectral sensors installed in UAVs for overall mangrove canopy assessments. The discrimination between the two mangrove species is possible with a simple decision tree analysis among the UAV-VARI intervals extracted from the GEE-VARI series. For instance, we found that *Rhizophora mangle* leaves appear in dark green, whereas *Avicennia germinans* emerge with bright and grayish-green colors. This color pattern was also found by Krause et al. (2004) in mangroves of northern Brazil. Although there is no published work on the use of the VARI index for mangrove forest classification, the feasibility of such data is not surprising because results from studies in precision agriculture have already published useful findings by means of a similar platform, sensor, and analysis (e.g., Zhang et al., 2019).

4.3. Mangrove forest canopy recovery

As to *Rhizophora mangle* defoliation and early signs of recovery, the results of our study indicated that only 21% of the original fringe canopy

remained one month after the landfall of Hurricane Willa. However, there was a 1.7-fold increase between 2018 and 2019, and a 1.2-fold in 2020, reaching an overall 53% of the original canopy cover in 2021. This pattern is relatively similar to that found by Kennedy et al. (2020), who recorded a substantial number of seedlings established five weeks after the landfall of a hurricane. Despite this initial recovery, several more years will perhaps be required to determine if the mangrove system is similar to conditions before the hurricane struck. In this sense, Radabaugh et al. (2020) found that after an initial increase from 40% canopy in the first two months following Hurricane Irma's landfall, there was an additional 60% canopy cover after six months post-storm in mangroves of Florida. Nevertheless, the authors indicated that there was mortality post-storm after nine months. Jamaluddin et al. (2021) analyzed the same hurricane category 3 (Irma) and, using Sentinel-2 data, found that only ~27% of the mangrove was degraded, while the rest remained intact. McCarthy et al. (2021) analyzed the same hurricane with 91 WorldView-2 images encompassing seven years before and one year after the impact and found that only 17% of the mangrove was degraded and, from this percentage, 35% recovered one year after Hurricane Irma's landfall. Imbert (2018) mentions that the fringe and shrub mangrove stands had not recovered to pre-hurricane conditions after 23 years from the impact of Hurricane Hugo. Han et al. (2018) mention that the decreased mangrove area recovered to a pre-hurricane condition in 3–4 years. According to Rivera-Monroy et al. (2019), it took almost ten years for a mangrove forest to recover after the impact of Hurricane Wilma in Florida. The extension of the mangrove defoliation damage and rate of re-establishment thus seemingly depends on local environmental conditions. Hence, our results indicate that the semi-arid mangroves of Marismas Nacionales were more severely damaged by a similar category 3 hurricane.

4.4. Environmental implications

The results of the time series analysis show a tendency towards the recovery of the mangrove cover area. This pattern agrees with the results found in the orthomosaics, which, unlike satellite images, can determine the fragmentation of the mangrove canopy to a greater degree (Fraser and Congalton, 2018) and thus predict how long it would take for it to recover. Based on the linear tendency, it will take at least 8.5 years for the mangrove cover area to reach its original size. However, this does not mean that the vertical canopy structure will recuperate in that time. It should be kept in mind that a mangrove tree takes longer to develop large and long branches compared to the initial leaf growth on branches that survived after a hurricane impact (Jamaluddin et al., 2021). Since the growth meristem is destroyed in thin branches compared to thick trunks, the early sign of recovery means that mangroves tend to develop leaves on the lower part of the trunk when they are under stressful conditions (Flores-de-Santiago et al., 2012). Imbert (2018) observed that the mechanism of regrowth from damaged trees is common in *Avicennia germinans* and *Laguncularia racemosa*, but not in *Rhizophora mangle*. This is a direct defense mechanism of mangroves because the frequency of hurricanes is one of the main factors limiting mangrove growth and contributing to mangrove canopy height configuration (Radabaugh et al., 2020). These mechanisms have severe implications regarding post-storm assessments. For instance, Kovacs et al. (2009) mention that a classification misconception occurs when authors only focus on change detection techniques within the overall mangrove cover area rather than analyzing the variability in the vertical composition. In this sense, some defoliated trees could have 13-m heights, although they started developing leaves in the understory, which could be quantified using satellite images and confused as restoration, even if the height of the original canopy had not been nearly as close to its pre-hurricane configuration. Flores-de-Santiago et al. (2017) indicated that stressed *Rhizophora mangle* seedlings needed nine years to reach their maximum height of only 4 m in an area north of the study site. Therefore, the overall change in the vertical canopy configuration will depend on local conditions. Environmental conditions are another factor to consider. For example, the 13-m high pre-storm fringe *Rhizophora mangle* trees of Marismas Nacionales are diminutive compared to riverine mangroves located in more favorable conditions, allowing them to reach heights of up to 60 m (Simard et al., 2019). Ultimately, the effects of defoliation and degradation of the vertical structure of the canopy and the time required to recover will depend on the specific location, mangrove species, and the intensity of the hurricane.

5. Conclusions

In October 2018, Hurricane category 3 Willa made landfall on the coastal zone of Marismas Nacionales, Mexico, and caused substantial mangrove defoliation and fragmentation. We examined the feasibility of quantifying mangrove canopy damage and early signs of recovery by using time series analysis of VI from the GEE platform and a consumer-grade UAV. Our approach was relatively simple: it was based on freely available satellite data, using built-in cameras of commercial UAVs. This was thus a relatively inexpensive complementary method for ground-based mangrove assessments. Although this study demonstrates the feasibility of the VARI index on mangrove forest discrimination, additional research is needed to evaluate our findings at various sites worldwide and with different mangrove species. The advantage of using UAVs relies on their capacity to assess detailed canopy damage and vertical canopy configuration due to their ultra-high spatial resolution (cm/pixel). Results from this study provide the first quantitative evidence that the use of the VARI index and decision tree classification is a particularly important advantage over previous approaches that have utilized manual classification, which is a time-consuming approach. Overall, there was a 78% canopy loss of the *Rhizophora mangle* one month after the landfall of Hurricane Willa. However, there was also a 1.7-fold increase in the canopy after one-year post-storm, which eventually reached 53% of the original canopy three years after the impact. The linear model shows a prediction of at least 8.5 years to reach pre-impact mangrove cover conditions. Nevertheless, the sequence of DSM estimates that the vertical canopy configuration will require a longer time to achieve its original structure. Importantly, we suggest that not all sites of Marismas Nacionales may recover into a similar mangrove forest because of differences in environmental conditions and mangrove species composition. In addition to a methodological summary, this study sheds light on various challenges and opportunities associated with the further development of UAV-based mangrove monitoring. We thus hope that this study will contribute to complementary approaches for environmental assessments of mangrove forests in other parts of the world.

Author statement

DAVM: Methodology, Software, Data curation. **FFdS**: Conceptualization, Data curation, writing review & editing, Funding acquisition. **LVL**: Methodology, Software. **DS**: Methodology, Data curation, Software. **RRS**: Data curation, Software. **LFAS**: Data curation, Software. **FFV**: Validation, Supervision, fieldwork, Funding acquisition. All authors read and approved the final manuscript.

Declaration of competing interest

The authors declare that they have no known competing financial interests or personal relationships that could have appeared to influence the work reported in this paper.

Acknowledgements

This research was funded by the Programa de Apoyo a Proyectos de Investigación e Innovación Tecnológica (Mexico) under Grants numbers IA100218 and IA100521 awarded to FFdS. Additional funding for the

field work was provided through the Instituto de Ciencias del Mar y Limnología (Mexico) under Grants numbers 622 and 323 awarded to FFdS and FFV, respectively. Dr. Leonardo Moroyoqui-Rojo of ECOSS Restauraciones Ambientales (Mexico) provided logistical support in the field campaigns. This article is dedicated to the memory of Dr. Manuel Blanco y Correa of Universidad Autónoma de Nayarit (Mexico). Guillermina Fehér edited the English text.

References

Arreola-Lizárraga, J.A., Flores-Verdugo, F.J., Ortega-Rubio, A., 2004. Structure and litterfall of an arid mangrove stand on the Gulf of California, Mexico. Aquat. Bot. 79, 137–143. https://doi.org/10.1016/j.aquabot.2004.01.012.

Ávila-Flores, G., Juárez-Mancilla, J., Hinojosa-Arango, G., Cruz-Chávez, P., López-Vivas, J.M., Arizpe-Covarrubias, O., 2020. A practical index to estimate mangrove conservation status: the forests from La Paz Bay, Mexico as a case study. Sustainability 12 (858). https://doi.org/10.3390/su12030858.

Bashan, Y., Moreno, M., Salazar, B.G., Alvarez, L., 2013. Restoration and recovery of hurricane-damaged mangroves using the knickpoint retreat effect and tides as dredging tools. J. Environ. Manag. 116, 196e203. https://doi.org/10.1016/j.jenvman.2012.11.045.

Bendig, J., Yu, K., Aasen, H., Bolten, A., Bennertz, S., Broscheit, J., Gnyp, M.L., Bareth, G., 2015. Combining uav-based plant height from crop surface models, visible, and near infrared vegetation indices for biomass monitoring in barley. Int. J. Appl. Earth Obs. Geoinf. 39, 79–87. https://doi.org/10.1016/j.jag.2015.02.012.

Calderon, R., Navas-Cortes, J.A., Lucena, C., Zarco-Tejada, P.J., 2013. High-resolution airborne hyperspectral and thermal imagery for early, detection of verticillium wilt of olive using fluorescence, temperature and narrow-band spectral indices. Remote Sens. Environ. Times 139, 231–245. https://doi.org/10.1016/j.rse.2013.07.031.

Cao, J., Leng, W., Liu, K., Liu, L., He, Z., Zhu, Y., 2019. Object-based mangrove species classification using unmanned aerial vehicle hyperspectral images and digital surface models. Rem. Sens. 10 (89) https://doi.org/10.3390/rs10010089.

Diniz, C., Cortinhas, L., Nerino, G., Rodrigues, J., Sadeck, L., Adami, M., Souza-Filho, P. W.M., 2019. Brazilian mangrove status: three decades of satellite data analysis. Rem. Sens. 11, 808. https://doi.org/10.3390/rs11070808.

Doyle, T.W., Smith III, T.J., Robblee, M.B., 1995. Wind damage effects of hurricane Andrew on mangrove communities along the southwest coast of Florida, USA. J. Coast Res. 21, 159–168. http://www.jstor.org/stable/25736006.

Du, M.M., Noguchi, N., 2017. Monitoring of wheat growth status and mapping of wheat yield's within-field spatial variations using color images acquired from uav-camera system. Rem. Sens. 9 (289) https://doi.org/10.3390/rs9030289.

Félix-Pico, E.F., Holguín-Quiñones, O.E., Hernández-Herrera, A., Flores-Verdugo, F., 2006. Mangrove primary production at El Conchalito estuary in La Paz (Baja California Sur, Mexico). Cienc. Mar. 32 (1A), 53–63. https://doi.org/10.7773/cm.v32i1.65.

Feller, I.C., Dangremond, E.M., Devlin, D.J., Lovelock, C.E., Proffitt, C.E., Rodriguez, W., 2015. Nutrient enrichment intensifies hurricane impact in scrub mangrove ecosystems in the Indian River Lagoon, Florida, USA. Ecology 96 (11), 2960–2972. https://doi.org/10.1890/14-1853.1.

Fickert, T., 2020. To plant or not to plant, that is the question: reforestation vs. natural regeneration of hurricane-disturbed mangrove forests in Guanaja (Honduras). Forests 11 (1068). https://doi.org/10.3390/f11101068.

Flores-de-Santiago, F., Valderrama-Landeros, L., Rodríguez-Sobreyra, R., Flores-Verdugo, F., 2020. Assessing the effect of flight altitude and overlap on orthoimage generation for UAV estimates of coastal wetlands. J. Coast Conserv. 24 (35) https://doi.org/10.1007/s11852-020-00753-9.

Flores-de-Santiago, F., Kovacs, J.M., Flores-Verdugo, F., 2018. Discrimination of 3 dominant mangrove species from the Pacific coast of Mexico by spectroscopy on intact leaves. Cienc. Mar. 44 (3), 185–202. https://doi.org/10.7773/cm.v44i3.2806.

Flores-de-Santiago, F., Serrano, D., Flores-Verdugo, F., Monroy-Torres, M., 2017. Application of a simple and effective method for mangrove afforestation in semiarid regions combining nonlinear models and constructed platforms. Ecol. Eng. 103, 244–255. https://doi.org/10.1016/j.ecoleng.2017.04.008.

Flores-de-Santiago, F., Kovacs, J.M., Lafrance, P., 2013a. An object-oriented classification method for mapping mangroves in Guinea, West Africa, using multipolarized ALOS PALSAR L-band data. Int. J. Remote Sens 34 (2), 563–586. https://doi.org/10.1080/01431161.2012.715773.

Flores-de-Santiago, F., Kovacs, J.M., Flores-Verdugo, F., 2013b. The influence of seasonality in estimating mangrove leaf chlorophyll-a content from hyperspectral data. Wetlands Ecol. Manage 21, 193–207. https://doi.org/10.1007/s11273-013-9290-x.

Flores-de-Santiago, F., Kovacs, J.M., Flores-Verdugo, F., 2012. Seasonal changes in leaf chlorophyll a content and morphology in a sub-tropical mangrove forest of the Mexican Pacific. Mar. Ecol. Prog. Ser. 444, 57–68. https://doi.org/10.3354/meps09474.

Flores-Verdugo, F., Ramírez-Barrón, E., Flores-de-Santiago, F., 2018. Hydroperiod enhancement using underground pipes for the efficient removal of hypersaline conditions in a semiarid coastal lagoon. Continent. Shelf Res. 162, 39–47. https://doi.org/10.1016/j.csr.2018.04.008.

Flores-Verdugo, F., Gonzalez-Farias, F., Zamorano, D.S., Ramirez-Garcia, P., 1992. Mangrove ecosystems of the Pacific Coast of Mexico: distribution, structure, litterfall, and detritus dynamics. Coastal Plant Community Lat. Am. 17, 269–288. https://doi.org/10.1016/B978-0-08-092567-7.50023-4.

Flores-Verdugo, F.J., Day, J.M., Briseño-Dueñas, R., 1987. Structure, litter fall, decomposition, and detritus dynamics of mangroves in a Mexican coastal lagoon with an ephemeral inlet. Mar. Ecol. Prog. Ser. 35, 83–90.

Fraser, B.T., Congalton, R.G., 2018. Issues in unmanned aerial systems (UAS) data collection of complex forest environments. Rem. Sens. 10 (908). http://doiorg/10.3390/rs10060908.

Gao, Q., Yu, M., 2022. Evaluating regimes modulated the responses of canopy structure of coastal mangrove forests to hurricane damage. Rem. Sens. 14 (1497) https://doi.org/10.3390/rs14061497.

George, S.L., Balasubramani, K., Shekhar, S., Venkatesham, E., Prasad, K.A., Grover, A., Mahata, D., Kumar, A., Ashique, V.V., Libina, R.S., Swaminathan, D.R., Balasundareshwaran, A., Annaidasan, K., 2021. A comprehensive study on preparedness, impact, response and recovery from tropical severe cyclonic storm 'GAJA': lessons for the future. J. Coast Conserv. 25 (58) https://doi.org/10.1007/s11852-021-00842-3.

Gitelson, A.A., Gritz, Y., Merzlyak, M.N., 2003. Relationship between leaf chlorophyll content and spectral reflectance and algorithms for non-destructive chlorophyll assessment in higher plant leaves. J. Plant Physiol. 160, 271–282. https://doi.org/10.1078/0176-1617-00887.

Gitelson, A.A., Kaufman, Y.J., Stark, R., Rundquist, D., 2002. Novel algorithms for remote estimation of vegetation fraction. Rem. Sens. Environ. 80, 76–87. https://doi.org/10.1016/S0034-4257(01)00289-9.

Gitelson, A., Merzlyak, M.N., 1994. Spectral reflectance changes associated with autumn senescence of Aesculus hippocastanum L. and Acer platanoides L. leaves. Spectral features and relation to chlorophyll estimation. J. Plant Physiol. 143 (3), 286–292. https://doi.org/10.1016/s0176-1617(11)81633-0.

Guerrero, J.M., Pajares, G., Montalvo, M., Romeo, J., Guijarro, M., 2012. Support vector machines for crop/weeds identification in maize fields. Expert Syst. Appl. 39, 11149–11155. https://doi.org/10.1016/j.eswa.2012.03.040.

Guo, Q., Su, Y., Hua, T., Zhao, X., Wu, F., Li, Y., Liu, J., Chen, L., Xu, G., Lin, G., Zheng, Y., Lin, Y., Mi, X., Fei, L., Wang, X., 2017. An integrated UAV-borne lidar system for 3D habitat mapping in three forest ecosystems across China. Int. J. Rem. Sens. 38 (8–10), 2954–2972. https://doi.org/10.1080/01431161.2017.1285083.

Gupta, K., Mukhopadhyay, A., Giri, S., Chanda, A., Datta Majumdar, S., Samanta, S., Mitra, D., Samal, R.N., Pattnaik, A.K., Hazra, S., 2018. An index for discrimination of mangroves from non-mangroves using LANDSAT 8 OLI imagery. MethodsX 5, 1129–1139. https://doi.org/10.1016/j.mex.2018.09.011.

Han, X., Feng, L., Hu, C., Kramer, P., 2018. Hurricane-induced changes in the Everglades National Park mangrove forest: Landsat observations between 1985 and 2017. J. Geophys. Res. Biogeosci 123, 3470–3488. https://doi.org/10.1029/2018JG004501.

Hatfield, J.L., Prueger, J.H., 2010. Value of using different vegetation indices to quantify agricultural crop characteristics at different growth stages under varying management practices. Rem. Sens. 2, 562–578. https://doi.org/10.3390/rs2020562.

Hunt, E.R., Daughtry, C., Eitel, J.U., Long, D.S., 2011. Remote sensing leaf chlorophyll content using a visible band index. Agron. J. 103 (4), 1090–1099. https://doi.org/10.2134/agronj2010.0395.

Imbert, D., 2018. Hurricane disturbance and forest dynamics in east Caribbean mangroves. Ecosphere 9 (7), e02231. https://doi.org/10.1002/ecs2.2231.

Jamaluddin, I., Thaipisutikul, T., Chen, Y.N., Chuang, C.H., Hu, C.L., 2021. MDPrePost-Net: a spatial-spectral-temporal fully convolutional network for mapping of mangrove degradation affected by hurricane Irma 2017 using Sentinel-2 data. Rem. Sens. 13 (5042) https://doi.org/10.3390/rs13245042.

Kennedy, J.P., Dangremond, E.M., Hayes, M.A., Preziosi, R.F., Rowntree, J.K., Feller, I. C., 2020. Hurricanes overcome migration lag and shape intraspecific genetic variation beyond a poleward mangrove range limit. Mol. Ecol. 1–15. https://doi.org/10.1111/mec.15513, 00.

Kovacs, J.M., Lu, X.X., Flores-Verdugo, F., Zhang, C., Flores de Santiago, F., Jiao, X., 2013. Applications of ALOS PALSAR for monitoring biophysical parameters of a degraded black mangrove (*Avicennia germinans*) forest. ISPRS J. Photogramm. Remote Sens 82, 102–111. https://doi.org/10.1016/j.isprsjprs.2013.05.004.

Kovacs, J.M., Liu, Y., Zhang, C., Flores-Verdugo, F., Flores de Santiago, F., 2011. A field based statistical approach for validating a remotely sensed mangrove forest classification scheme. Wetlands Ecol. Manage 19, 409–421. https://doi.org/10.1007/s11273-011-9225-3.

Kovacs, J.M., King, J.M.L., Flores-de-Santiago, F., Flores-Verdugo, F., 2009. Evaluating the condition of a mangrove forest of the Mexican Pacific based on an estimated leaf area index mapping approach. Environ. Monit. Assess. 157, 137–149. https://doi.org/10.1007/s10661-008-0523-z.

Kovacs, J.M., Blanco-Correa, M., Flores-Verdugo, F., 2001. A logistic regression model of hurricane impacts in the mangrove forest of the Mexican Pacific. J. Coast Res. 17 (1), 30–37. https://www.jstor.org/stable/4300147.

Krause, G., Bock, M., Weiers, S., Braun, G., 2004. Mapping land-cover and mangrove structures with remote sensing techniques: a contribution to a synoptic GIS in support of coastal management in North Brazil. Environ. Manage 34 (3), 429–440. https://doi.org/10.1007/s00267-004-0003-3.

Krauss, K.W., Osland, M.J., 2020. Tropical cyclones and the organization of mangrove forests: a review. Ann. Bot. 125, 213–234. https://doi.org/10.1093/aob/mcz161.

Li, Z., Zan, Q., Yang, Q., Zhu, D., Chen, Y., Yu, S., 2019. Remote estimation of mangrove aboveground carbon stock at the species level using a low-cost unmanned aerial vehicle system. Rem. Sens. 11 (1018) https://doi.org/10.3390/rs11091018.

Liu, X., Wang, L., 2018. Feasibility of using consumer-grade unmanned aerial vehicles to estimate leaf area index in Mangrove forest. Remote Sens. Lett. 9 (11), 1040–1049. https://doi.org/10.1080/2150704X.2018.1504339.

Liu, H., Zhang, K., Li, Y., Xie, L., 2013. Numerical study of the sensitivity of mangroves in reducing storm surge and flooding to hurricane characteristics in southern Florida. Continent. Shelf Res. 64, 51–65. https://doi.org/10.1016/j.csr.2013.05.015.

Mafi-Gholami, D., Zenner, E.K., Jaafari, A., Ward, R.D., 2019. Modeling multi-decadal mangrove leaf area index in response to drought along the semi-arid southern coasts of Iran. Sci. Total Environ. 656, 1326–1336. https://doi.org/10.1016/j.scitotenv.2018.11.462.

McCarthy, M.J., Jessen, B., Barry, M.J., Figueroa, M., McIntosh, J., Murray, T., Schmid, J., Muller-Karger, F.E., 2021. Automated high-resolution time series mapping of mangrove forests damaged by hurricane Irma in southwest Florida. Rem. Sens. 12 (1740) https://doi.org/10.3390/rs12111740.

Muro-Torres, V., Soto-Jiménez, M., Green, M.F., Quintero, L., Amezcua, F., 2019. Food web structure of a subtropical coastal lagoon. Aquat. Ecol. 53, 407–430. https://doi.org/10.1007/s10452-019-09698-0.

Neupane, B., Horanont, T., Hung, N.D., 2019. Deep learning based banana plant detection and counting using high-resolution red-green-blue (RGB) images collected from unmanned aerial vehicle (UAV). PLoS ONE. 14(10), e0223906. https://doi.org/10.1371/journal.pone.0223906.

Nóbrega, G.N., Ferreira, T.O., Neto, M.S., Queiroz, H.M., Artur, A.G., Mendonca, E.D.S., Silva, E.D.O., Otero, X.L., 2016. Edaphic factors controlling summer (rainy season) greenhouse gas emissions (CO_2 and CH_4) from semiarid mangrove soils (NE-Brazil). Sci. Total Environ. 542, 685–693. https://doi.org/10.1016/j.scitotenv.2015.10.108.

Oldeland, J., Revermann, R., Luther-Mosebach, J., Buttschardt, T., Lehmann, J.R.K., 2020. New tools for old problems — comparing drone- and field-based assessments of a problematic plant species. Environ. Monit. Assess. 193 (90) https://doi.org/10.1007/s10661-021-08852-2.

Otero, V., Van de Kerchove, R., Satyanarayana, B., Martínez-Espinosa, C., Amir Bin Fisol, M., Bin Ibrahim, M.R., Sulong, I., Mohd-Lokman, H., Lucas, R., Dahdouh-Guebas, F., 2018. Managing mangrove forests from the sky: forest inventory using field data and unmanned aerial vehicle (UAV) imagery in the Matang mangrove forest reserve, peninsular Malaysia. Forest Ecol. Manag. 411, 35–45. https://doi.org/10.1016/j.foreco.2017.12.049.

Peereman, J., Hogan, J.A., Lin, T.C., 2022. Disturbance frequency, intensity and forest structure modulate cyclone-induced changes in mangrove forest canopy cover. Global Ecol. Biogeography 31, 37–50. https://doi.org/10.1111/geb.13407.

Pennings, S.C., Glazner, R.M., Hughes, Z.J., Kominoski, J.S., Armitage, A.R., 2021. Effects of mangrove cover on coastal erosion during a hurricane in Texas, USA. Ecol. 102(4), e03309. https://doi.org/10.1002/ecy.3309.

Radabaugh, K.R., Moyer, R.P., Chappel, A.R., Dontis, E.E., Russo, C.E., Joyse, K.M., Bownik, M.W., Goeckner, A.H., Khan, N.S., 2020. Mangrove damage, delayed mortality, and early recovery following hurricane Irma at two landfall sites in Southwest Florida, USA. Estuar. Coast 43, 1104–1118. https://doi.org/10.1007/s12237-019-00564-8.

Rivera-Monroy, V.H., Danielson, T.M., Castañeda-Moya, E., Marx, B.D., Travieso, R., Zhao, X., Gaiser, E.E., Farfan, L.M., 2019. Long-term demography and stem productivity of Everglades mangrove forests (Florida, USA): resistance to hurricane disturbance. Forest Ecol. Manage 440, 79–91. https://doi.org/10.1016/j.foreco.2019.02.036.

Rouse, J.W., Haas, R.H., Schell, J.A., Deering, D.W., 1973. Monitoring vegetation systems in the great plains with ERTS (Earth resources technology satellite). In: Proceedings of 3rd Earth Resources Technology Satellite Symposium. Greenbelt, pp. 309–317, 10–14 December, SP-351.

Ruwaimana, M., Satyanarayana, B., Otero, V., Muslim, A.M., Syafiq, M., Ibrahim, S., Raymaekers, D., Koedam, N., Dahdouh-Guebas, F., 2018. The advantages of using drones over space-borne imagery in the mapping of mangrove forests. PLos ONE. 13 (7), e0200288. https://doi.org/10.1371/journal.pone.0200288.

Saenger, P., 2002. Mangrove Ecology, Silviculture and Conservation. Kluwer Academic Publishers, Dordrecht.

Serrano, D., Flores-Verdugo, F., Ramírez-Félix, E., Kovacs, J.M., Flores-de-Santiago, F., 2020. Modeling tidal hydrodynamic changes induced by the opening of an artificial inlet within a subtropical mangrove dominated estuary. Wetlands Ecol. Manage 28, 103–118. https://doi.org/10.1007/s11273-019-09697-w.

Serrano-Rubio, J.P., Ruiz, M.D.M., Vidal-Espitia, U., 2021. Integrating remote sensing and image processing to test for disturbance effects in a post-hurricane mangrove ecosystem. Signal Image Video Process 15, 351–359. https://doi.org/10.1007/s11760-020-01754-9.

Shi, T., Liu, J., Hu, Z., Liu, H., Wang, J., Wu, G., 2016. New spectral metrics for mangrove forest identification. Remote Sens. Lett. 7, 885–894. https://doi.org/10.1080/2150704X.2016.1195935.

Simard, M., Fatoyinbo, L., Smetanka, C., Rivera-Monroy, V.H., Castañeda-Moya, E., Thomas, N., Van der Stocken, T., 2019. Mangrove canopy height globally related to precipitation, temperature and cyclone frequency. Nat. Geosci. 12, 40–45. https://doi.org/10.1038/s41561-018-0279-1.

Sona, G., Pinto, L., Pagliari, D., Passoni, D., Gini, R., 2014. Experimental analysis of different software packages for orientation and digital surface modelling from UAV images. Earth Sci. Info 7 (2), 97–107. https://doi.org/10.1007/s12145-013-0142-2.

Stary, K., Jelinek, Z., Kumhalova, J., Chyba, J., Balazova, K., 2020. Comparing RGB-based vegetation indices from UAV imageries to estimate hops canopy area. Agron. Res. 18 (4), 2592–2601. https://doi.org/10.15159/AR.20.169.

Tomlinson, P.B., 1994. The Botany of Mangroves. Cambridge University Press, Cambridge.

Torres-Sanchez, J., Pena, J.M., de Castro, A.I., Lopez-Granados, F., 2014. Multi-temporal mapping of the vegetation fraction in early season wheat fields using images from uav. Comput. Electron. Agric. 103, 104–113. https://doi.org/10.1016/j.compag.2014.02.009.

Valderrama-Landeros, L., Flores-Verdugo, F., Rodríguez-Sobreyra, R., Kovacs, J.M., Flores-de-Santiago, F., 2021. Extrapolating canopy phenology information using Sentinel-2 data and the Google Earth Engine platform to identify the optimal dates for remotely sensed image acquisition of semiarid mangroves. J. Environ. Manag. 279 (111617) https://doi.org/10.1016/j.jenvman.2020.111617.

Valderrama-Landeros, L., Blanco-y-Correa, M., Flores-Verdugo, F., Álvarez-Sánchez, L.F., Flores-de-Santiago, F., 2020. Spatiotemporal shoreline dynamics of Marismas Nacionales, Pacific coast of Mexico, based on a remote sensing and GIS mapping approach. Environ. Monit. Assess. 192 (123) https://doi.org/10.1007/s10661-020-8094-8.

Valderrama-Landeros, L., Flores-de-Santiago, F., 2019. Assessing coastal erosion and accretion trends along two contrasting subtropical rivers based on remote sensing data. Ocean Coast Manag. 169, 58–67. https://doi.org/10.1016/j.ocecoaman.2018.12.006.

Valderrama-Landeros, L., Flores-de-Santiago, F., Kovacs, J.M., Flores-Verdugo, F., 2018. An assessment of commonly employed satellite-based remote sensors for mapping mangrove species in Mexico using an NDVI-based classification scheme. Environ. Monit. Assess. 190 (23), 1–12. https://doi.org/10.1007/s10661-017-6399-z.

Walcker, R., Laplanche, C., Herteman, M., Lambs, L., Fromard, F., 2019. Damages caused by hurricane Irma in the human-degraded mangroves of Saint Martin (Caribbean). Sci. Rep. 9 (18971) https://doi.org/10.1038/s41598-019-55393-3.

Wan, L., Li, Y.J., Cen, H.Y., Zhu, J.P., Yin, W.X., Wu, W.K., Zhu, H.Y., Sun, D.W., Zhou, W.J., He, Y., 2018. Combining uav-based vegetation indices and image classification to estimate flower number in oilseed rape. Rem. Sens. 10 (1484) https://doi.org/10.3390/rs10091484.

Wang, D., Wan, B., Liu, J., Su, Y., Guo, Q., Qiu, P., Wu, X., 2020. Estimating aboveground biomass of the mangrove forests on northeast Hainan Island in China using an upscaling method from field plots, UAVLiDAR data and Sentinel-2 imagery. Int. J. Appl. Earth Obs. Geoinformation 85 (101986). https://doi.org/10.1016/j.jag.2019.101986.

Woebbecke, D.M., Meyer, G.E., Vonbargen, K., Mortensen, D.A., 1995. Color indexes for weed identification under various soil, residue, and lighting conditions. Trans. ASAE (Am. Soc. Agric. Eng.) 38, 259–269.

Xie, B., Yang, W.N., Wang, F., 2020. A new estimate method for fractional vegetation cover based on uav visual light spectrum. Sci. Surv. Mapp. 45, 72–77.

Yao, Q., Liu, K., Wu, Y., Aragon-Moreno, A.A., Rodrigues, E., Cohen, M., de Souza, A.V., Farfan, L.M., Antinao, J.L., 2021. A multi-proxy record of hurricanes, tsunami, and post-disturbance ecosystem changes from coastal southern Baja California. Sci. Total Environ. 796 (149011) https://doi.org/10.1016/j.scitotenv.2021.149011.

Yu, X., Liu, Q., Liu, X., Liu, X., Wang, Y., 2017. A physical-based atmospheric correction algorithm of unmanned aerial vehicles images and its utility analysis. Int. J. Rem. Sens. 38 (8–10), 3101–3112. https://doi.org/10.1080/01431161.2016.1230291.

Zhang, J., Virk, S., Porter, W., Kenworthy, K., Sullivan, D., Schwartz, B., 2019. Applications of unmanned aerial vehicle based imagery in turfgrass field trials. Front. Plant Sci. 10 (279) https://doi.org/10.3389/fpls.2019.00279.

Zhang, C., Kovacs, J.M., Liu, Y., Flores-Verdugo, F., Flores-de-Santiago, F., 2014. Separating mangrove species and conditions using laboratory hyperspectral data: a case study of a degraded mangrove forest of the Mexican Pacific. Rem. Sens. 6, 11673–11688. http://dx.di.org/10.3390/rs61211673.

Zhou, R., Yang, C., Li, E., Cai, X., Yang, J., Xia, Y., 2021. Object-based wetland vegetation classification using multi-feature selection of unoccupied aerial vehicle RGB imagery. Rem. Sens. 13 (4910) https://doi.org/10.3390/rs13234910.

Zhu, X., Hou, Y., Weng, Q., Chen, L., 2019. Integrating UAV optical imagery and LiDAR data for assessing the spatial relationship between mangrove and inundation across a subtropical estuarine wetland. ISPRS J. Photogramm. Remote Sens 149, 146–156. https://doi.org/10.1016/j.isprsjprs.2019.01.021.

Zhu, Y., Liu, K., Liu, L., Myint, S.W., Wang, S., Liu, H., He, Z., 2017. Exploring the potential of WorldView-2 Red-Edge band-based vegetation indices for estimation of mangrove leaf area index with machine learning algorithms. Rem. Sens. 9 (1060) https://doi.org/10.3390/rs9101060.